Magnet fall inside a conductive pipe: motion and the role of the pipe wall thickness

2009 Eur. J. Phys. 30 855

(http://iopscience.iop.org/0143-0807/30/4/018)

IOP PUBLISHING EUROPEAN JOURNAL OF PHYSICS

Eur. J. Phys. **30** (2009) 855–869 doi:10.1088/0143-0807/30/4/018

Magnet fall inside a conductive pipe: motion and the role of the pipe wall thickness

G Donoso, C L Ladera and P Martín

Departamento de Física, Universidad Simón Bolívar, Apdo. 89000, Caracas 1080, Venezuela

E-mail: clladera@usb.ve and pmartin@usb.ve

Received 12 February 2009, in final form 25 March 2009
Published 27 May 2009
Online at stacks.iop.org/EJP/30/855

Abstract

Theoretical models and experimental results are presented for the retarded fall of a strong magnet inside a vertical conductive non-magnetic tube. Predictions and experimental results are in good agreement modelling the magnet as a simple magnetic dipole. The effect of varying the pipe wall thickness on the retarding magnetic drag is studied for pipes of different materials. Conductive pipes of thinner walls produce less dragging force and the retarded fall of the magnet is seen to consist of an initial transient accelerated regime followed by a stage of uniform motion. Alternative models of the magnet field are also presented that improve the agreement between theory and experiments.

(Some figures in this article are in colour only in the electronic version)

1. Introduction

Magnetic braking of a falling magnet inside a non-magnetic conductive pipe [1–3] and the Thomson jumping ring [4, 6] are experiments frequently shown in lecture demonstrations, in open-day physics shows and in science museum exhibits. Both experiences are interesting and capture the students' and public imagination, but they are also difficult for anyone to give a formal account. The subject of magnetic braking indeed attracts attention and has been addressed in scientific journals a number of times [1–3, 7, 8]. Magnetic braking has also found a number of important applications in the present technology [9]. Both the jumping ring [4, 6] and the vertical motion of a small magnet inside a conductive tube are manifestations of Faraday magnetic induction and have recently begun to be studied thoroughly in the laboratory [1–3] because of their pedagogical value. It offers, for instance, a good opportunity for a very low cost, honours degree or senior undergraduate experiment on Faraday induction, and it is also an excellent case for illustrating the modelling of an intriguing physics phenomenon.

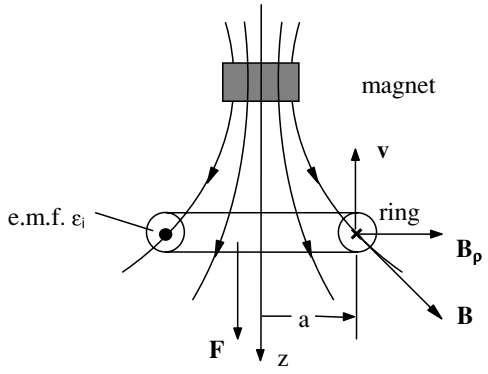

Figure 1. A conductive ring moves with speed **v** along the magnet main symmetry axis, in the non-uniform magnetic field **B** of the magnet. An opposing force **F** and an induced e.m.f appear in the ring.

The magnetic drag force on a strong magnet falling inside a vertical conductive tube is re-examined here with the idea of exploring new ground, particularly from the experimental side. The phenomenon is just another example of a body that falls under the action of a retarding force, sky-divers and the remarkable 'flying' seeds of some trees [10], also being cases of motion under the action of retarding forces. In such phenomena, the bodies begin falling in transient accelerated motion, a regime that soon yields to uniform motion under the combined action of the gravitational force and a retarding force. The constant speed in such final motion is the so-called *terminal speed*. Below, the pertinent equations of the magnet motion are derived from a new electromagnetic perspective using a rather simple physics model, and the role of the thickness of the pipe wall is examined, both experimentally and theoretically, for different materials. The influence of the pipe wall thickness has not been addressed in previous works, or at least not with the detail presented here. The results of a set of experiments with pipes of different wall thicknesses and diameters, and two different materials, aluminium and copper, are reported in order to check the validity of the models proposed here.

1.1. The models

Consider a short conductive ring moving in a region where a non-uniform magnetic field exists; two main effects can be observed (figure 1). Firstly, a variable retarding magnetic force **F** appears on the short ring opposing its motion; secondly, a transient induced electro-motive force (e.m.f.) ε_i is induced in the ring. As already noted in a previous work [3], a relevant axial symmetry exists between the induced effects on the conductive ring and those on the magnetic object that generates the field.

The equivalent symmetry found in the interaction of a magnet—that falls inside along the longitudinal pipe axis—and an infinitesimal conductive ring defined in the pipe wall is exploited below. Both of these interactions are manifestations of magnetic induction, and their mathematical representation can be obtained by applying Faraday's law of induction. It is relatively easy to derive expressions for both the magnitude of the magnetic dragging force F on the magnet and the induced e.m.f. ε_i on the infinitesimal conductive ring. For a small ring of radius a (figure 1) moving with a small velocity **v** in the field **B** of a magnet, the induced e.m.f. is given [11] by

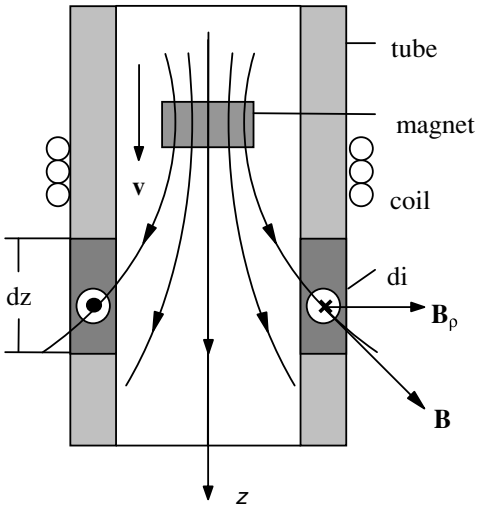

Figure 2. Longitudinal cross-section of a magnet falling inside a conductive tube. A circular current d*i* is induced in the pipe as the magnet falls down with velocity **v.** A coil of thin wires, wrung onto the pipe, measures the induced e.m.f. in the pipe

$$\varepsilon_i = \int (\overline{v} \times \overline{B}) \cdot \overline{\mathrm{d}l} = v B_\rho (2\pi a), \tag{1}$$

where B_ρ is the radial component of the magnetic field, and the integral was evaluated along the ring. The axial force component F_z opposing the motion of the ring along the z-axis is

$$F_z = \mathrm{i}(\overline{l} \times \overline{B})_z = 2\pi \mathrm{i} a B_\rho. \tag{2}$$

For a disc-shaped magnet that falls inside a conductive pipe, the field **B** is produced by the magnet itself and (in the light of the symmetry mentioned above) we consider a small motionless element of the pipe in the shape of a ring of length dz (figure 2) of internal and external radii a and b, equal to the pipe radii. This ring transports an induced electric current di due to the changing magnetic flux across it. It is thus necessary to obtain an expression for the magnetic field produced by the magnet.

This field **B** can be initially approximated as being produced by a simple magnetic dipole. In spherical coordinates (r, φ, θ), the expressions for the radial and co-latitude components, B_r and B_θ, of the dipole field are given [12, 13] by

$$B_r = 2\mu \frac{\cos\theta}{r^3}, \qquad B_\theta = \mu \frac{\sin\theta}{r^3}, \tag{3}$$

where μ is the magnitude of the magnetic dipole moment of the magnet. In our case, it is convenient to change the reference coordinates to a set of cylindrical ones (ρ, ϕ, z), where the z-axis is the pipe axis; then, the axial component B_z and the radial component B_ρ of the field are respectively given by

$$B_z = B_r \cos\theta - B_\theta \sin\theta = \frac{\mu}{(\rho^2 + z^2)^{5/2}} \left[\frac{3z}{\rho^2 + z^2} - 1 \right], \tag{4}$$

$$B_\rho = B_r \sin\theta + B_\theta \cos\theta = \frac{3\mu z \rho}{(\rho^2 + z^2)^{5/2}}. \tag{5}$$

Inserting the latter expression in equation (1), we get for the induced e.m.f. ε_i,

$$\varepsilon_i = v(2\pi\, a)\frac{3\mu\, z\, a}{(a^2+z^2)^{5/2}}. \tag{6}$$

If σ is the conductivity of the material of the pipe wall and dA denotes the cross-sectional area of a small ring element—of length $l = 2\pi a$—then the conductance of this ring is dC = $\sigma\,\mathrm{d}A/l$, and the induced current di along such a ring can be expressed as

$$\mathrm{d}i = \varepsilon_i\,\mathrm{d}C = \varepsilon_i\frac{\sigma\,\mathrm{d}A}{l} = B_\rho\; v\sigma\;\mathrm{d}A. \tag{7}$$

Denoting with e the pipe thickness, the magnetic force dF on the small ring of height dz is given by

$$\mathrm{d}F = l\,B_\rho\,\mathrm{d}i = (2\pi a)\,B_\rho^2\sigma\, ve\,\mathrm{d}z \tag{8}$$

or

$$\mathrm{d}F = (2\pi a^2)\sigma\, ve\left(\frac{3\mu}{a^3}\right)^2\frac{u^2\,\mathrm{d}u}{(1+u^2)^5}, \tag{9}$$

where we have resorted to equation (5) and introduced the new variable u with $z = au$.

Applying the principle of action and reaction, the latter expression is seen to represent the force that the infinitesimal pipe ring exerts on the magnet falling along the longitudinal axis of the pipe. Integrating equation (9) along the pipe then gives the effective retarding force on the magnet,

$$F = \int_{-\infty}^{\infty}(2\pi a^2)\sigma\, ve\left(\frac{3\mu}{a^3}\right)^2\frac{u^2\,\mathrm{d}u}{(1+u^2)^5} = (2\pi a^2)\sigma\, ve\left(\frac{3B_0}{2}\right)^2\frac{f}{\pi}, \tag{10}$$

where f is a constant obtained by evaluating the integral on the variable u on the left-hand side of equation (10), namely

$$f = \int_{-\infty}^{\infty}\frac{u^2\,\mathrm{d}u}{(1+u^2)^5} = \frac{5\pi}{256}. \tag{11}$$

A single value of the magnet field, $B_0 = 2\mu/z_0^3$, has been introduced in equation (10). This B_0 is just a convenient value: it is the magnetic field at the axial point of coordinate z_0, measured from the magnet centre. Moreover, note that the integral in equation (11) can be calculated in several ways, for instance, using a mathematical computer software package. The field value B_0 can also be experimentally measured (see section 4).

The magnetic dragging force on the magnet is finally given by equations (10) and (11) as

$$F = \left(\frac{36\pi f\sigma e\,\mu^2}{a^4}\right)v \equiv kv, \tag{12}$$

where k is given by

$$k = \frac{36\pi f\sigma e\,\mu^2}{a^4}, \tag{13}$$

a constant that represents the *magnetic dragging*, or 'damping' on the magnet motion, produced by the Foucault currents induced in the pipe.

2. Magnetic braking force and the terminal speed of the magnet

If m is the mass of the falling magnet, then its motion, due to its weight mg and the magnetic braking force F, is given by Newton's second law as

$$m\left(\frac{\mathrm{d}v}{\mathrm{d}t}\right) = mg - F = mg - kv, \tag{14}$$

where k is the constant given in equation (13). The solution to this differential equation—after separation of the variables v and t—gives the varying speed $v(t)$ of the falling magnet inside the pipe as

$$v(t) = \frac{\mathrm{d}z}{\mathrm{d}t} = v_T[(1 - \exp(-t/\tau)], \tag{15}$$

where the time constant τ and constant speed v_T are given by

$$\tau = \frac{m}{k}, \tag{16}$$

and

$$v_T = \frac{mg}{k}. \tag{17}$$

As in many cases of motion of a body, under the combined action of a retarding force and a constant force, the magnet motion consists of an initial short duration transient regime followed by uniform terminal motion, where the constant speed is precisely the terminal speed v_T given by equation (17). It will be shown below that the experiments accurately reproduce the predictions of our theoretical model. Finally, the vertical position $z(t)$ of the magnet is then obtained from the expression for $v(t)$ in equation (15) as

$$z(t) = v_T\tau\left[\frac{t}{\tau} - 1 + \exp(-t/\tau)\right]. \tag{18}$$

Note that for $t \gg \tau$, the vertical position is simply given by

$$z(t) = v_T(t - \tau), \tag{19}$$

which represents a straight line in the (t, z) coordinate plane.

3. Preliminary measurements and experiment set-up

A single cylindrical rare earth SmCo strong magnet, 12.5 mm in diameter and 3.2 mm long, was used in all the experiments. The mass of this magnet is 3.0 g. A set of nine 15 cm long tubes of different diameters and wall thicknesses—five of them made of copper and four of aluminium—were machined down in the workshop from 1 inch diameter solid bars. The inner diameter of all the tubes is 13.8 mm, their external diameters being 15.8, 18.0, 20.0, 22.0 and 25.4 mm, respectively, in the case of the copper ones. A wider 56 cm long copper pipe, 18.7 mm in internal diameter, was also procured from stock, to perform additional experiments to check our magnetic dipole model of the strong magnet. To measure the conductivity of the material of the tubes, their electrical resistance was measured using a variable current source—good enough to provide 0–50 A at 0–20 V—and two high-accuracy digital multimeters. For instance, the characteristics of the wider and longer copper pipe were found to be as follows: length 56 cm, internal diameter 18.7 $\pm$ 0.05 mm, wall thickness $e = 1.74 \pm 0.02$ mm and electrical resistance $R = 0.140 \pm 0.005$ mΩ. From such data, the conductivity of the material of our wider and longer tube was found to be $\sigma = (3.58 \pm 0.18) \times 10^7\ \Omega^{-1}\ \mathrm{m}^{-1}$. This is only 62% of the currently accepted conductivity of pure copper

($\sigma_{Cu} = 5.92 \times 10^7\ \Omega^{-1}\ m^{-1}$) because the material of this tube is not pure copper. The conductivity of the shorter tubes was found to be very close to the conductivity of pure copper.

Pick-up coils, of either 10 or 20 turns, made of a thin copper wire were wrung onto the outer cylindrical surface of each tube (see figure 2). These coils were closely packed onto the surface of the tubes. As explained in a previous work [3], such coils can be used to detect the magnet falling along the tube, by monitoring the transient e.m.f. induced in them. Such a transient signal can be easily displayed on the screen of a modern low-cost digital oscilloscope and even stored in its permanent memory. The temporal dependence of such a transient resembles an anti-symmetric dispersion curve, and its central zero-crossing point can be used to find the time when the magnet crosses the pick-up coil mid-plane. It has been found that this experimental procedure, for measuring the effect on the pipe by the passing magnet, gives reliable transit times of the magnet at the pick-up coils, and no other procedures are needed. The accurate values of the instantaneous speed can be derived from the signals of two pick-up coils located a small distance apart. Moreover, plotting the magnet *position* z versus time t curve, it is possible to find accurate values of two of the three characteristic constants of the phenomenon being studied: the terminal speed v_T and the time constant τ (see equations (17) and (18)). These constants can be assessed by measuring the slope of the asymptote at infinite time to the plotted curve of the magnet's vertical position z versus t (as in figure 7), and finding the value at which such an asymptote cuts the t-axis.

For numerical convenience, we introduced in section 2 a magnetic induction value B_0 at the point of coordinate z_0 located on the main axis of symmetry of the disc magnet. To measure this B_0 value, a calibrated axial Hall probe was used. Alternatively, the field value B_0 can be estimated by measuring the peak value of the transient e.m.f. induced in a given pick-up coil by the passing magnet. In effect, such maximum amplitude of the transient allows one to determine the magnetic dipole moment μ of the falling magnet, and from such a dipole moment one can then obtain the required B_0 by applying the well-known dipolar approximation relation $\mu = 2B_0\, {z_0}^3$. Thus, for $z_0 = 9.5$ mm, and using one of the transient curves, we obtained $\mu = 4.7 \times 10^{-8}$ T m^3 which gave $B_0 = 0.11$ T. The values of B_0 obtained using this experimental procedure gave consistent results that also agreed with the value of the field at $z = z_0$ measured using the Hall probe.

We may expect that the transient induced e.m.f. signal captured by a pick-up coil wrung onto the external face of the tube, as the magnet passes by, should give a good representation of the radial component B_ρ of the magnetic induction. In effect, from equation (6),

$$\varepsilon_i = N\ v B_\rho (2\pi\, a) = N\ v\ (2\pi\, a) \left(\frac{3\mu z a}{(a^2 + z^2)^{5/2}} \right). \tag{20}$$

In the case of the narrower tubes, the stationary regime of the observed descent is quickly reached by the magnet as it moves down, and then we can replace the speed v in the latter equation by the terminal, or limit, magnet speed v_T. By the same token, we can approximate the vertical position z of the magnet by equation (19), $z = v_T(t - \tau)$, where τ is the time constant. Once v_T and τ are known, one can then plot the e.m.f. ε_i against the vertical position z of the falling magnet by using equation (20). This plot is shown in figure 3, together with the experimental data points of the induced e.m.f.s. It may be seen that the two plots show almost the same profile and maxima, but that they somehow depart for the larger values of z. In section 7, we shall present a new way to model the magnet (the *planar loop* model) which gives a much better approximation to the experimentally obtained data generated by the magnet.

Our theoretical model also allows us to predict values for the three main constants of the phenomenon. For a copper tube of internal mean radius $a = 9.50$ mm, thickness $e = 1.24$ mm,

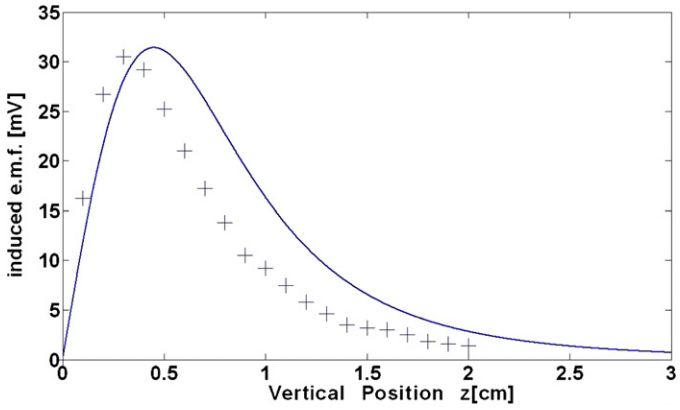

Figure 3. Induced electro-motive force e.m.f. (mV) in a pick-up coil, by a magnet that falls along a copper tube, plotted as a function of the vertical position z (cm) of the magnet from the coil. The continuous trace has been plotted using the magnetic dipole approximation. The crosses represent the experimental data.

conductivity $\sigma = 5.92 \times 10^7\ \Omega^{-1}\ \mathrm{m}^{-1}$, and a magnet of mass $m = 3.0$ g, we predict an axial value of the field $B_0 = 0.11$ T (gravity acceleration $= 9.80\ \mathrm{m\ s}^{-2}$). Our equations in section 2 then give the following motion constant values:

$$k = F/v = 0.11\ \mathrm{N/(m/s)}, \qquad \tau = 0.0418\ \mathrm{s}, \tag{21}$$

and $v_T = 0.410\ \mathrm{m\ s}^{-1}$. These are very good predictions as the experiments later revealed (see section 5).

4. The role of the pipe thickness and the *effective thickness*

In section 2, we obtained a valid expression, equation (12), for the magnetic braking force on a strong small magnet falling inside a tube by using Faraday's induction law and the magnet dipole approximation. An implicit assumption made is that the thickness e of the cylindrical wall is much smaller than the pipe's inner radius a, i.e. $e \ll a$. Instead, we may consider a pipe of finite thickness $e = b - a$, where b is the external radii of the pipe. A tube of infinitesimal thickness da exerts on the falling magnet an infinitesimal force dF given by equation (9),

$$\mathrm{d}F = \left(\frac{36\pi f \sigma v \mu^2}{a^4}\right) \mathrm{d}a. \tag{22}$$

Integrating across the wall, i.e. from a to b, we get a new expression for the magnetic braking force,

$$F = \int_a^b \frac{36\pi f \sigma v \mu^2}{a'^4}\, \mathrm{d}a' = \frac{36\pi f \sigma v \mu^2}{3}\left(\frac{1}{a^3} - \frac{1}{b^3}\right). \tag{23}$$

Introducing the *thickness parameter* λ defined so that $b = \lambda\, a$, the latter equation becomes

$$F = \frac{36\pi f \sigma\ v \mu^2}{a^4}\frac{a}{3}\left(1 - \frac{1}{\lambda^3}\right). \tag{24}$$

It is therefore useful to define the *effective thickness* e' of the cylindrical wall as

$$e' = \frac{a}{3}\left(1 - \frac{1}{\lambda^3}\right) \quad \Leftrightarrow \quad \frac{e'}{a} = \frac{1}{3}\left(1 - \frac{1}{\lambda^3}\right). \tag{25}$$

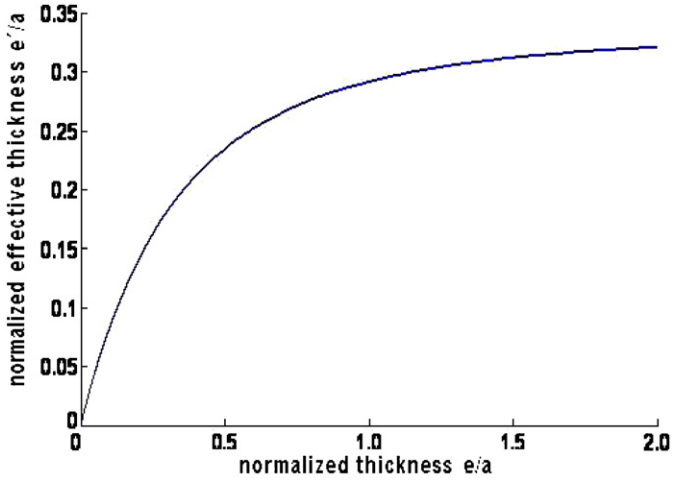

Figure 4. Normalized effective thickness e'/a of a conductive tube, of inner radius a, plotted against the actual thickness e/a of the tube.

Table 1. Thickness parameter (λ) and the effective thickness e'/a, for given values of the true thickness e/a of the copper tubes (a is the internal diameter of the tubes).

λ	e/a	e'/a
1	0	0
1.17	0.17	0.123
1.20	0.20	0.140
1.40	0.40	0.212
1.60	0.60	0.252
1.80	0.80	0.276
2.00	1.00	0.292
3.00	2.00	0.320
∞	∞	0.333

This effective thickness e' has to be replaced above in all the relations where the pipe thickness e appears. For instance the magnetic drag constant k in equation (13) should be rewritten as

$$k = \frac{36\pi f \sigma e' \mu^2}{a^4} = \frac{36\pi f \sigma \mu^2}{a^4} \frac{a}{3} \left(1 - \frac{1}{\lambda^3}\right). \tag{26}$$

Table 1 shows a set of values of the thickness parameter λ and the corresponding values of the ratio e/a, and for comparison the values of the ratio e'/a. A plot of the values of the ratio e'/a versus e/a is shown in figure 4.

5. Experiments and results

A set of experiments were prepared and performed to test the theory of magnetic braking presented above. The copper and aluminium tubes made in the workshop and mentioned in section 4 were used. A set of no less than 30 cylindrical pick-up coils made of a thin copper wire, of different diameters and different number of turns, were wrung and arranged coaxially

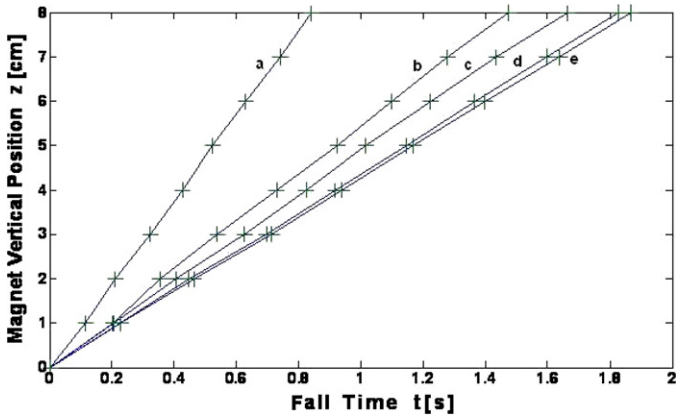

Figure 5. Vertical position of the magnet, as a function of time t, falling inside five copper tubes of increasing wall thickness: (a) 1.0 mm, (b) 2.10 mm, (c) 3.10 mm, (d) 4.10 mm and (e) 5.80 mm. The slope of each plot gives the terminal speed of the magnet motion under the force of gravity and the magnetic drag force.

along a single vertical axis. The coils, exchangeable between the tubes, were placed, with constant vertical separations, either around the conductive pipes to monitor the fall of the magnet inside the pipes, or simply arranged vertically to monitor the magnet-free fall in air.

In the first experiments, we let the strong magnet fall inside each of the five short copper tubes of different thicknesses. To avoid magnetic border effects, the first and last coils were placed 4 cm from the ends of each tube, thus ensuring that the currents induced in the tube were always symmetrical with respect to the coil mid-planes. Figure 5 shows the magnet vertical position as a function of time for the five copper tubes of different thickness (denoted a to e, respectively, in the figure).

Nine coils, placed at 1 cm intervals, were used to detect the magnet falling down the tubes. Almost straight lines can be fitted to the experimental points in figure 5, and their slopes represent the terminal speeds of the falling magnet under the magnetic retarding force. As expected, the greater the wall thickness of a pipe the lower the magnet terminal speed. In effect, equation (10) of our theoretical model, which assumes a thin-walled tube, shows that the magnetic braking constant k is proportional to the thickness e of the surrounding conductive pipe, and equation (18) shows that the terminal speed is inversely proportional to that constant. Therefore, we expect the disc magnet to fall at lower speeds as the pipe wall thickness increases. This is just a natural consequence of the Faraday and Lenz laws: greater wall thickness means larger induced Foucault currents in the pipe and therefore a larger opposing force on the magnet. Moreover, note that in the case of short and narrower tubes, the dragging magnetic force is large enough to make the falling magnet reach the terminal speed in a period of time so short (at most of the order of 0.01 s) that the plots in figure 5 look like simple straight lines, the transient accelerated fall regime 'hidden' in a small neighbourhood at $t = 0$. In contrast, the data from the experiments done with a longer, larger diameter tube do show the transient accelerated regime of the magnet fall, as the magnetic retarding force is not so strong (see figure 8).

In figure 5, the two extreme plots, (a) and (e), correspond to tubes of wall thicknesses of 1.0 mm and 5.8 mm, respectively. The slopes of such plots differ roughly by a factor of about 2, while in accordance with equations (13) and (17), they should differ by a larger factor (approximately 6). The reason for the divergence of course lies in the finite thickness of the pipe walls. It may be seen in figure 4 that the normalized effective thicknesses of the 1.0 mm

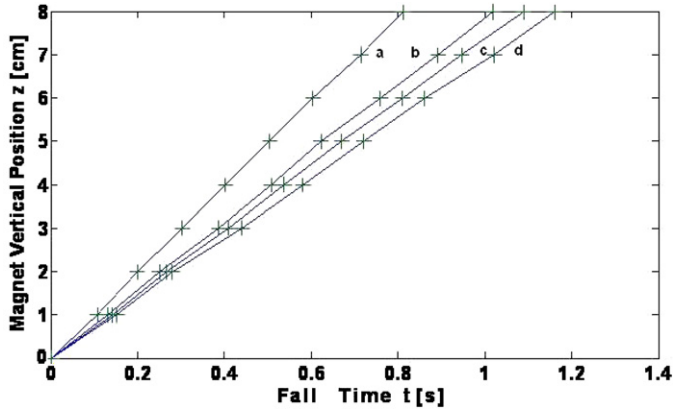

Figure 6. Vertical position of the magnet as a function of time t, as it falls inside four aluminium tubes of increasing wall thicknesses: (a) 2.10 mm, (b) 3.10 mm, (c) 4.10 mm and (d) 5.80 mm. The slope of each plot gives the terminal speed of the magnet motion under the force of gravity and the magnetic dragging force.

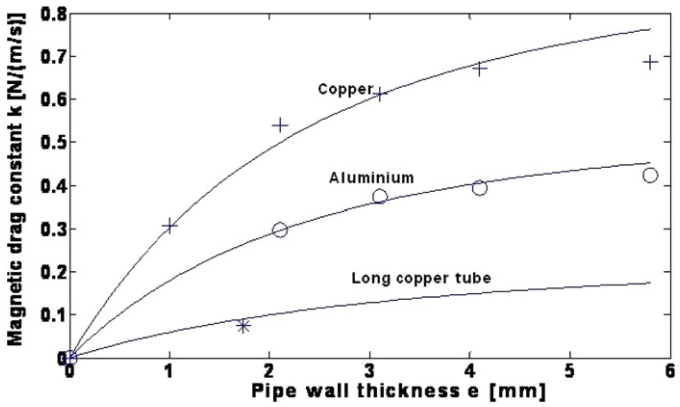

Figure 7. Magnetic drag constant k (N/(m/s)) versus the thickness e (mm) of tube walls: copper (upper trace: crosses) and aluminium tubes (middle trace: circles). The lower trace corresponds to a 56 cm long copper tube and has been obtained using equation (19). The point (*) plotted at $e = 1.74$ mm is the experimental value of the magnetic drag constant of this long tube.

and 5.8 mm thick tubes are 0.128 and 0.257, respectively, whose ratio is about 2 as it should be if the theoretical model correctly predicts the results in figure 5.

Figure 6 shows our laboratory results using the four aluminium tubes. Again, the plots are almost straight lines and represent the terminal speeds inside each tube. The speed decreases as the thickness of the tube wall increases. The slopes of the plots are larger than those in the case of copper tubes (note the difference in the abscissa scale between the two figures). This is expected since the conductivity of aluminium, being only 0.6 times that of copper, implies less dragging force on the magnet.

In figure 7, the magnetic dragging constant k is plotted against the actual wall thicknesses of the copper and aluminium tubes. The plots are obtained after finding the terminal speed, and the time constant τ, using the data plotted in figures 5 and 6. The upper plot corresponds to the copper tubes while the middle curve belongs to the aluminium tubes. The third curve in the figure comes from the application of our theoretical model to the single 58 cm long copper

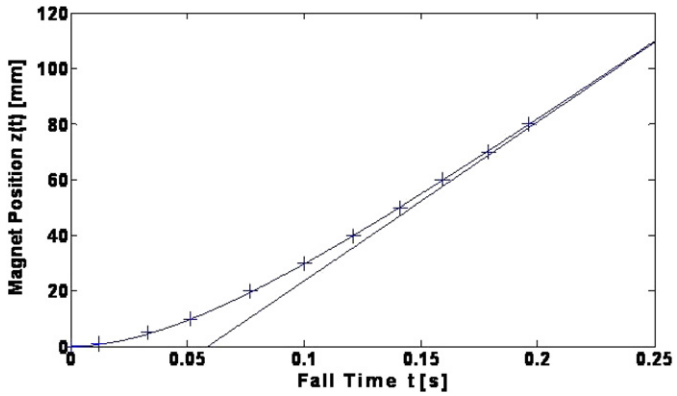

Figure 8. The magnet's vertical position z as a function of time t as it falls along a 56 cm long copper tube. Experimental data are plotted with crosses. The curve corresponds to our theoretical model. The slope of the asymptote to the trace, at large values of t, represents the terminal speed of the magnet. Note the transient accelerated regime of the magnet for values of time less than $t \approx 0.1$ (s).

tube whose inner diameter is 18.7 mm (wall thickness of 1.74 mm) used in our experiments. This larger diameter copper pipe produces a smaller retarding force on the falling magnet, as expected. The isolated single experimental point (*) of coordinates (1.74 mm, 0.075 N/(m/s)), plotted in the figure, represents the magnetic constant k of the longer copper pipe.

Finally, in figure 8, the vertical position of the falling magnet is plotted as a function of time for the long wider copper pipe, i.e. z versus t. Note the excellent agreement between the theoretical curve given by equation (18) and our experimental data. The motion of the magnet is plotted in a short range of time, but long enough to make clearly visible the initial transient accelerated motion of the magnet before it reaches its terminal speed, as a consequence of the opposing weight and variable magnetic drag. Also plotted in the figure appears the asymptote (for large values of the time t) to the magnet position curve. The abscissa $t = 0.0589$ s where the asymptote cuts the time axis is just the time constant τ of the magnet motion inside the longer copper tube. Note that for this copper tube, the transient accelerated regime of the magnet lasts for about 0.1 s, at least one order of magnitude larger than that in the case of the narrower 15 cm long conductive tubes. This transient regime does not last as long in the case of the narrower tubes, whose magnetic retarding constants are two or three times larger than those in the case of the 56 cm long, larger internal diameter, copper pipe as shown in figure 7. Also note that the terminal speed of the magnet is about $v_t = 0.5$ m s^{-1}. Note that the two measured constants of this long tube $\tau = 0.0589$ s and $v_t = 0.5$ m s^{-1} are of the same order of the theoretical predictions we made at the end of section 4.

6. The *planar loop* or Biot–Savart approximation and the scaled dipole approximation

In section 2, we found discrepancies between the actual induced e.m.f. in the walls of a conductive tube and the falling magnet induced e.m.f. predicted by our model (figure 3). The discrepancies are: (i) a small difference in the height of the maximum given by the model and that given by the data points, (ii) the maxima occur at different abscissae and (iii) the width of the theoretical curve is larger than the width of the trace obtained with the actual experimental points. Our model, we recall, is based on the simple dipole approximation, and therefore we may conclude that such a simple approximation is lacking. Let us begin, first of all, with

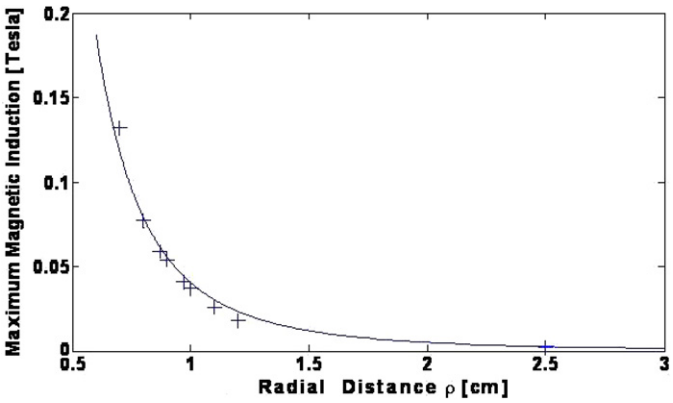

Figure 9. Maximum values of the radial component of the magnetic induction of a disc magnet, as it falls inside a conductive tube, plotted as a function of the radius of pick-up coils wrung onto the tube. The crosses are experimental data points obtained from the maxima of the e.m.f. induced in the tube wall.

the possible mismatch between the heights of the two maxima of the induced e.m.f. ε_i in figure 3: these heights, for data points and theory, should be the same. Note that equation (1) shows that the induced e.m.f. ε_i is simply proportional to the radial component B_ρ of the magnetic induction. So one looks for the dependence of the maximum of such a radial component upon the radial direction (ρ) of the conductive tube, which happens to be the radial direction of the pick-up coils wrung onto the tubes. Applying the procedure to find a maximum, one gets after differentiating equation (6) and using equation (1), the expression that gives the maximum height of the radial component B_ρ as a function of the magnetic dipole μ:

$$B_{\rho,\max} = \left(\frac{48\mu}{25\sqrt{5}}\right)\frac{1}{a^3}. \tag{27}$$

This maximum occurs for the vertical position $z = a/2$, where a is the radius of the given pick-up coil used to detect the falling magnet. In figure 9, the maxima $B_{\rho,\max}$ is plotted against the radii a of the pick-up coils using equation (27), and for a magnetic dipole value $\mu = 4.716 \times 10^{-8}\,\mathrm{T\,m^3}$. The latter corresponds to the typical value $B_0 = 0.11$ T of the magnetic induction produced by our disc magnet, at the axial distance $z = a_0 = 9.5$ mm from the centre of the magnet. Also plotted in figure 9 is the experimentally obtained set of maximum values $B_{\rho,\max}$. Note the good match of the experimental points and the curve obtained from our model (even for a coil of 25 mm radius). That is, the magnetic dipole approximation gives at least the correct height of the maxima of the radial component B_ρ and the induced e.m.f. ε_i, since both are just proportional (equation (1)).

To account for the other discrepancies in figure 3, already mentioned above, two new approximations are hereby introduced: first the so-called *planar loop approximation*, and then what we call the *abscissa-scaled dipole approximation*. The purpose of the new approximations is to get a better match between laboratory results and the theoretical model. The first new approximation is based on a well-known application of the Biot–Savart law of electromagnetism to the magnetic induction produced by a loop of current resting on a plane [14, 15]. The second new approximation arises from a simple inspection of figure 3. It simply consists in introducing a scale factor α in the z-abscissa axis: a change from z to αz. This simple scaling procedure, as shall be seen below, does not alter at all the key and basic

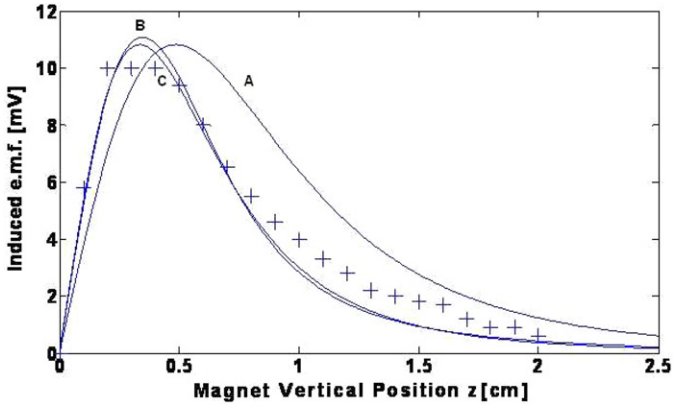

Figure 10. Induced e.m.f. as a function of the vertical position of a falling magnet inside a tube, the magnet being modelled as (A) a magnetic dipole, (B) a planar loop and (C) using the scaled-abscissa dipole approximation. The crosses represent the data points from experiments.

predictions concerning the motion of the magnet (for instance, the dragging constant already found above stays the same and so all predictions about the magnet motion).

The Biot–Savart law of electromagnetism can be applied to find the components B_ρ of the magnetic induction produced by a *loop of current* of radius a_{loop} resting on a plane. The well-known result [14, 15] is a couple of equations for the radial and co-latitude components B_r and B_θ of the induction in terms of the Legendre polynomials $P_{2n+1}(\cos\theta)$ and the associated Legendre polynomials, respectively. We have used those equations, expanded to the first order, to get the following new expression for the component $B_\rho\,(z,\,\rho)$ of the induction produced by our disc magnet:

$$B_\rho(z,\,\rho) = \frac{3\,\mu\,z\rho}{(z^2+\rho^2)^{5/2}}\left[1 - \frac{3}{8}\frac{a_{\text{loop}}^2}{(z^2+\rho^2)}\left(\frac{25z^2}{z^2+\rho^2} - 13\right)\right]. \tag{28}$$

Note that the zeroth-order expansion of the new approximation (the first term in the square bracket above) reproduces correctly our previous result (equation (5)) given by the dipole approximation. Assuming, once again, that for our magnet $\mu = 4.716 \times 10^{-8}$ T m^3, equations (28) and (1), can now be used to find the new expression for the induced e.m.f as a function of the vertical coordinate z, and the result appears plotted (curve marked B) in figure 10, jointly with the induced e.m.f. result predicted by the magnetic dipole approximation (curve A). The agreement between the experimental data and the curve obtained using the planar loop approximation is good, and certainly much better than that in figure 3.

Finally, the abscissa z in figure 3 can be scaled by multiplying it by an adjustable factor α, which leads to a new expression for the induced e.m.f., and for the radial component of the induction field. This third approximation may be called the *abscissa-scaled dipole approximation*. With this change, we get a new expression for the radial component of the magnet field

$$B_\rho = \frac{3\mu(\alpha\,z)\rho}{[(\alpha\,z)^2+\rho^2]^{5/2}}. \tag{29}$$

This approximation is simpler than the previous one since the appropriate value of the parameter α is simply the factor by which the dipole approximation overestimates the abscissa of the maximum of B_ρ with respect to the abscissa of the maximum given by the data points in

figure 3. It is important to note that neither the height of the maximum $B_{\rho,\max}$ nor the integral in equation (11) (leading to the magnetic drag force) is affected by scaling the abscissae with the scaling factor α. That is, this scaling of the abscissa z in figure 3 is far from being a convenient numerical trick to fit the experimental data. Our laboratory experiments revealed that the value of the scaling parameter α ranges from 1.2 for a coil of radius $a = 19.6$ mm to 1.5 for a coil of radius $a = 8.7$ mm.

7. Discussion

A new theoretical model to explain the retarded fall of a disc magnet inside a vertical conductive pipe has been presented, the magnet being modelled as a magnetic dipole. Three contributions of our model were presented: (i) the dependence of the magnetic drag constant upon the finite thickness of the pipe wall, (ii) accurate predictions for the dependence of the vertical descent of the magnet upon time and (iii) the explicit magnetic drag force on the magnet. Using a low-cost experimental set-up, and ordinary laboratory instruments such as multimeters and oscilloscopes, a large number of experiments were performed in the laboratory to confirm such contributions. Previous works, dealing with the current case of magnetic braking, have reported scarce or non-experimental results concerning the role of the thickness of the pipe walls. The conductive pipes in our experiments, of different wall thicknesses and made of two different readily available materials, allowed us to verify the dependence of the drag force on the conductivity of the material. Measurements using a longer, larger internal diameter, copper tube allowed us to observe the short transient accelerated regime, at the beginning of the magnet motion, and the motion evolution to the final motion stage with constant speed. Once again our model predictions were satisfactorily confirmed by the experimental results. In the first part of this work, the magnet was modelled as a magnetic dipole. Then a second, higher order approximation, based on the magnet modelled as a planar current loop, was also introduced in section 7, which led to better results. This second approximation, as expected, reduces to the dipole approximation, when taken at the zeroth order. A third approximation to the magnetic induction of the falling disc magnet based on a simple scaling of the vertical axis coordinate was also introduced in section 7. The three theoretical expressions for the radial component of the induction field, equations (5), (28) and (29), fail to reproduce the experiment results for vertical distances larger than the radius of the disc-shaped magnet; however, the magnet induction field in such a region of the z-axis contributes very little to the integral in equation (11) giving the magnetic drag force exerted by the tube on the magnet; therefore, we assert that the results obtained in this work are valid.

References

[1] Ireson G and Twidle J 2008 Magnetic braking revisited: activities for the undergraduate laboratory *Eur. J. Phys.* **29** 745–51
[2] Iñiguez J, Raposo V, Hernandez-Lopez A, Flores A G and Sazo M 2004 Study of the conductivity of a metallic tube by analysing the damped fall of a magnet *Eur. J. Phys.* **25** 37–9
[3] MacLachty C S, Backman P and Bogan L 1993 A quantitative magnetic braking experiment *Am. J. Phys.* **61** 1096–1106
[4] Tjossem P J H and Cornejo V 2000 Measurements and mechanisms of Thomson's jumping ring *Am. J. Phys.* **68** 238–44
[5] Bostock-Smith J M 2008 The jumping ring and Lenz's law—an analysis *Phys. Educ.* **43** 265–9
[6] Tanner P, Loebach J, Cook J and Hallen H D 2001 A pulsed jumping ring apparatus for demonstration of Lenz's law *Am. J. Phys.* **69** 911–6
[7] Wiederick H D, Gauthier N, Campbell D A and Rochon P 1987 Magnetic braking: simple theory and experiment *Am. J. Phys.* **55** 500–3
[8] Heald M A 1988 Magnetic braking: improved theory *Am. J. Phys.* **56** 521–2

[9] Tossman B E 1971 Variable parameter nutation damper for SAS-A *J. Spacecr. Rockets* **8** 743–6
[10] Ladera C L, Pineda P A and Alcala G 2000 Mechanical analysis of the dispersal flight of *Triplaris caracasana* Cham. *Ciencia* **8** 285–303
[11] Halliday D, Resnick R and Krane K S 1992 *Physics* vol 2 4th edn (New York: Wiley) chapter 36
[12] Wangsness R K 1981 *Electromagnetic Fields* (New York: Wiley) p 341
[13] Lorrain P and Corson D R 1970 *Electromagnetic Fields and Waves* 2nd edn (San Francisco: Freeman) pp 320–1
[14] Jackson J D 1975 *Classical Electrodynamics* 2nd edn (New York: Wiley) pp 177–80
[15] Arfken G B and Weber H J 1995 *Mathematical Methods for Physicists* 4th edn (San Diego, CA: Academic) pp 728–32